AIMS Materials Science, 3(1): 204-213.
DOI: 10.3934/matersci.2016.1.204
Received: 25 January 2016
Accepted: 19 February 2016
Published: 23 February 2016

http://www.aimspress.com/journal/Materials

Research article

Surface modification in mixture of ZnO + 3%C nanocrystals stimulated by mechanical processing

Tetyana Torchynska [1,*], Brenda Perez Millan [2], Georgiy Polupan [3], and Mykola Kakazey [4]

[1] ESFM – Instituto Politécnico Nacional, México D. F. 07738, MEXICO
[2] UPIITA – Instituto Politécnico Nacional, México D. F. 07320, MEXICO
[3] ESIME – Instituto Politécnico Nacional, México D. F. 07738, MEXICO
[4] CIICAp – Universidad Autónoma del Estado de Morelos, Cuernavaca, MEXICO

* **Correspondence:** Email: ttorch@esfm.ipn.mx.

Abstract: The photoluminescence (PL), Raman scattering and SEM images for the mixture of ZnO + 3% C nanocrystals (NCs) have been studied before and after of intensive mechanical processing (MP) with the aim to identify the nature of defects. The study reflects the diversity of physical processes occurring at MP: amorphizating the surface of ZnO NCs, crushing the individual ZnO NCs and carbon nanoparticles, covering the ZnO NC surface by the graphene layers, the oxidation partially of the graphene layers, carbon and ZnO NCs etc. Three stages of MP have been revealed which are accompanied by PL spectrum transformations: i) amorphizating the ZnO NC surface together with the generation of nonradiative recombination centers, ii) passivating the ZnO NC surface by the graphene layer with its oxidation partially and iii) further crushing of ZnO NCs, the oxidation of ZnO NCs and the formation of graphene (graphite) oxides. The new PL band peaked at 2.88 eV has been detected after 9 min of MP. Note that the passivation of the ZnO NC surface by graphene layer can be interesting for future technological applications.

Key words: ZnO nancrystals; graphene; graphene oxide; photoluminescence; Raman scattering

1. Introduction

ZnO nanocrystals (NCs) are characterized by the tuned electronic property, higher thermal

stability and oxidation resistance, compared with most other semiconductors [1]. Important properties have been revealed in the nanocrystallite composites ZnO + xC, which permits improving field emission of cathodes [2], engineering room-temperature ferromagnetism [3], modifying the luminescence properties [4], improving selective solar absorbed coatings [5]. Recently it was suggested that graphene-semiconductor nanostructures, such as Gr-ZnO, have shown improved optical switching and catalytic applications [6]. Obtaining the efficient ZnO optoelectronic devices requires the study of processes of the nonradiative and radiative defect generation in ZnO + xC NCs. The successful defect generation in ZnO at milling was demonstrated recently using EPR and photoluminescence methods [7]. At mechanical processing (MP) in a ball mill a big number of defects can be produced in ZnO NCs that permits to obtain the certain characteristics, which cannot be obtained in the defect-free crystals.

2. Materials and Method

The ZnO + 3%C mixtures, prepared from ZnO NCs (99.5% purity, Reasol; with the NC size of 200–600 nm) and carbon nanoparticles (EPRUI Nanoparticles & Microspheres Co. Ltd. with the size smaller ≤ 50 nm), were mixed in a ball mill (PM 400/2, Retsch Inc.) with the rotation speed of 400 rpm for the MP times 1, 3, 9 and 90 min. The grinding chamber of 50 ml with the tungsten carbide balls of the sizes: 3 of 20 mm and 10 of 10 mm has been used. The concentration of carbon (3%) in studied mixtures is chosen on the base of our previous study. It was shown early that carbon concentration increasing more than 3% in the ZnO + xC mixture was accompanied by decreasing the emission intensity owing to the essential absorption of ZnO emitting light in C nanoparticles.

PL spectra were measured at 300 K and the excitation by a He-Cd laser with a wavelength of 325 nm and a beam power of 46 mW using a PL setup on a base of spectrometer SPEX500 described in [8,9,10]. Raman scattering spectra were measured in the backscattering geometry in a Jobin-Yvon LabRAM HR 800UV micro-Raman system at the excitation by a LED with a light wavelength of 785 nm [11]. ZnO + 3%C NC images for different milling times have been obtained using the scanning electron microscopy (SEM) model Quanta 3D FEG-FEI.

3. Results

SEM images of ZnO + 3% C mixtures after various times of MP are presented in figure 1. ZnO NCs with the size within the range 200–600 nm have been seen clearly (Figure 1a). The amorphization of the ZnO NC surface at the start of milling (3–9 min) and the agglomerate formation have been revealed (Figure 1b, c). At long time of MP (90 min) the shape of majority ZnO NCs transforms and the agglomeration dominates in the ZnO NC ensembles (Figure 1c, d).

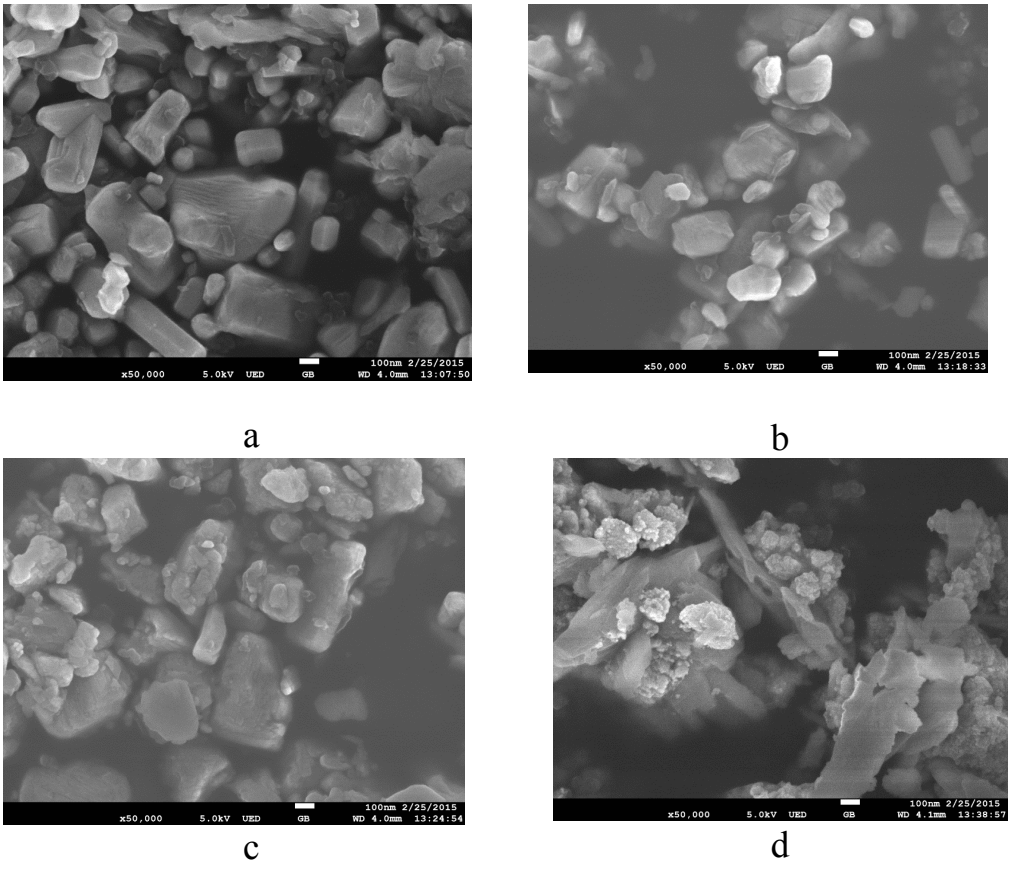

Figure 1. SEM images of ZnO + 3%C NCs for various milling times: 1 (a), 3 (b), 9 (c) and 90 min (d).

PL spectra of ZnO + 3%C mixtures measured at 300 K after various times of MP are shown in figure 2a,b. PL spectra are complex and can be represented as a set of PL bands. The deconvolution procedure (Figure 2c) has been applied to PL spectra that permit to obtain the Gaussian shape PL bands with the peaks at: 3.18 eV (A), 2.88 eV (B), 2.42 eV (C) and 2.12 eV (D). Integrated PL intensities, the half widths and PL peak positions have been estimated for all PL bands in an initial state and after various times of MP. The kinetics of integrated PL intensity variations versus MP times is presented in figure 3. As it is clear three stages exist in this kinetics (Figure 3). The PL intensity of UV and visible PL bands (A, C, D) decreases on the first MP stage (1–3 min). The kinetics slowing (Figure 3) and the new PL band peaked at 2.88 eV (B) has appeared on the second MP stage (3–9 min). At long time of MP (9–90 min) PL intensities of all bands (2.88, 2.42 and 2.12 eV) decrease together with shifting the peak of the PL band B to 2.85 eV (third MP stage).

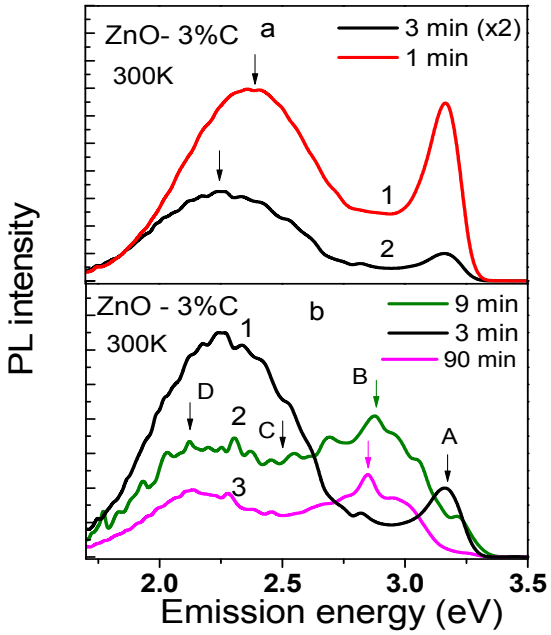

a, b

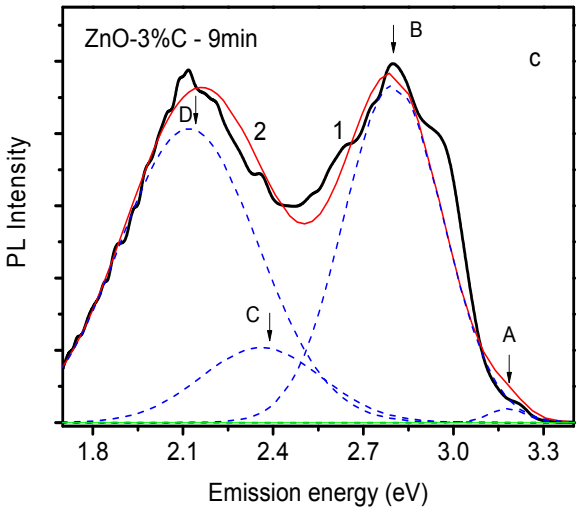

c

Figure 2. PL spectra measured after various MP times: (a) 1–1 min, 2–3 min, (b) 1–3 min, 2–9 min, 3–90 min. The PL intensity of the spectrum, measured after 3 min of MP, was multiplied on 2 in figure 2a. The deconvolution (c) of the PL spectrum (1), measured after 9 min of MP, on 4 elementary PL bands A, B, C, D and the PL intensity superposition (2) of these PL bands.

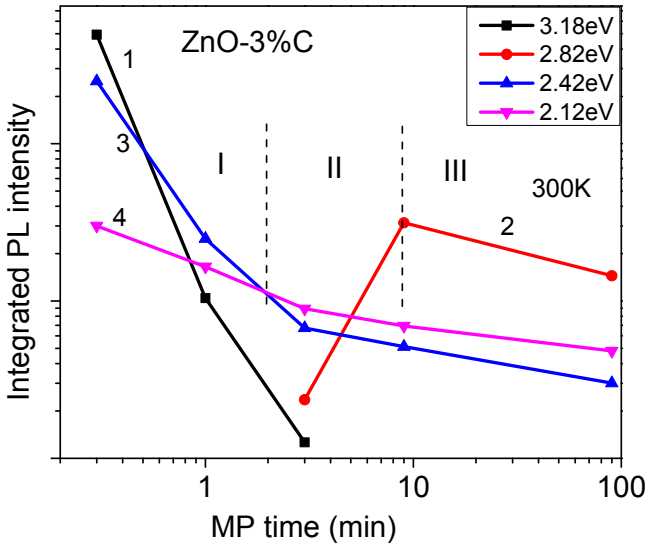

Figure 3. The variation of integrated PL intensities versus MP times.

Raman scattering spectra of ZnO + 3% C mixtures measured after various MP times are presented in figure 4. The Raman peaks at 194, 320 and 427 cm^{-1} related to scattering in ZnO NCs are detected for the Raman shifts of 80–500 cm^{-1} (Figure 4, Table 1). Positions of ZnO Raman peaks do not change at MP with an accuracy of 2 cm^{-1} (Table 1).

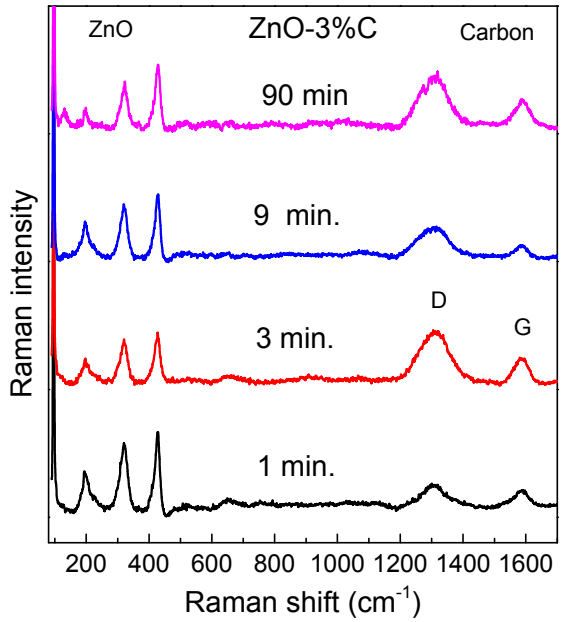

Figure 4. Raman scattering spectra measured after MP for: 1, 3, 9 and 90 min.

Table 1. Raman peaks detected in ZnO + 3%C mixtures before and after MP.

t_{MP}	n LA (cm^{-1})	$3E_{2H}$ - E_{2L} (cm^{-1})	E2 (high) (cm^{-1})	D band (cm^{-1})	G band (cm^{-1})
0 min	196	320	427	1306	1587
1 min	196	320	427	1306	1588
3 min	197	321	428	1311	**1588**
9 min	198	320	429	1306	**1580**
90 min	198	322	428	1308	**1582**

Raman peaks at 1306 (D) and 1587 (G) cm^{-1}, owing to Raman scattering in the carbon nanoparticles, have been revealed (Figure 4, Table 1). It is known that graphite has the Raman-active bands related to the vibrations of: i) the graphite lattice (G band) at 1575 cm^{-1} and ii) the graphite edges (D disordering band) at 1355 cm^{-1} [12,13]. It is known that disorder in graphite leads to the broader D and G band shapes and to higher D band relative intensity compared to that for a G band that we have seen in figure 4 for 3 min of MP. These changes testify on crushing the carbon (graphite) nanoparticles on the first MP stage. Then on the second MP stage (3–9 min) the Raman intensities of G and D bands a little bit decrease (Figure 4) together with the shift of D and G bands to lower frequencies down to 1306 and 1580 cm^{-1}, respectively (Table 1). At long time of MP (90min) the positions of G and D bands start to shift to higher frequencies (Table 1).

4. Discussion

UV and visible PL bands in ZnO are connected with the near-band-edge (NBE) and defect-related emissions, respectively [14]. NBE emission is attributed to the free or bound excitons, or to donor-acceptor pairs [14,15]. The high PL intensity and a small half width of 3.18 eV PL band (A) in the PL spectrum at 300K permit assigning this PL band to a LO phonon replica of free exciton emission in ZnO NCs.

PL intensity decreasing for NBE and defect-related PL bands on the first MP stage (1–3min) can be attributed to the generation of nonradiative recombination (NR) centers. NR center concentration increasing is accompanied by NR recombination rate rising together with falling down the PL intensity of UV and visible emissions. NR centers can be assigned to the dangling bonds on the ZnO NC surface created at surface amorphizating on the first MP stage.

PL intensity decay slowing on the second stage of MP that can be seen in figure 3. Simultaneously the new PL band, centered at 2.88 eV (B), appears in PL spectra (Figure 2b and Figure 3), and the PL band (D) dominates in the orange spectral range. At the same moment the G band in the Raman spectrum shifts to lower frequencies (Table 1).

Note that the G peak is located at a higher frequency (1593cm^{-1}) in graphite oxide (GO), but the G peak is located almost at the same frequency in single graphene sheets as that in graphite (1575–1580 cm^{-1}) [13]. Thus the shift of G band to 1580 cm^{-1} on the second MP stage testifies, apparently, that the single graphene layers have been formed on the surface of ZnO NCs. The

formation of graphene layers on the ZnO NC surface leads to passivating the NC surface together with the NR center annihilation. The last process is a reason of slowing the PL decay kinetics on the second MP stage.

Let us analyze the defect related PL bands in the mixture of ZnO + 3%C NCs. The PL band with the peak at 2.00–2.12 eV (orange) in ZnO was assigned early to the oxygen interstitial atoms (2.02 eV) [16] or to the hydroxyl group (2.10 eV) [17,18]. The PL band in the spectral range 2.40–2.50 eV (green) in ZnO was assigned to the oxygen vacancies [19], Cu impurities [20], zinc vacancies [21] or surface defects [19]. In studied mixtures the intensities of orange and green PL bands decrease at the first MP stage together with NBE emission (Figure 2b and 3). But at the end of first stage the orange PL band dominates in the PL spectrum. MP is carried out in ambient air and it is accompanied by temperature increasing the ZnO + 3% C mixture in a ball-mill chamber. These conditions are favorable for the ZnO NC oxidation additionally that can be accompanied by concentration increasing the oxygen interstitial atoms in ZnO and, as a result, slowing orange emission decay kinetics at MP.

The blue PL band with the peak at 2.80–2.90 eV in ZnO is attributed early to Cu related defects [19,22], to Zn interstitials [23] or to the donor–acceptor pairs included the shallow donor and oxygen vacancy [14,24]. The studied ZnO + 3% C mixtures do not content the Cu impurities. We cannot assign the defects responsible for the 2.88 eV PL band (B) to the oxygen vacancies or to the Zn interstitials taking into account the additional ZnO oxidation at MP. In our experiments the 2.88 eV PL band, apparently, can be assigned to emission of the graphene or graphite oxides [25,26] created at MP.

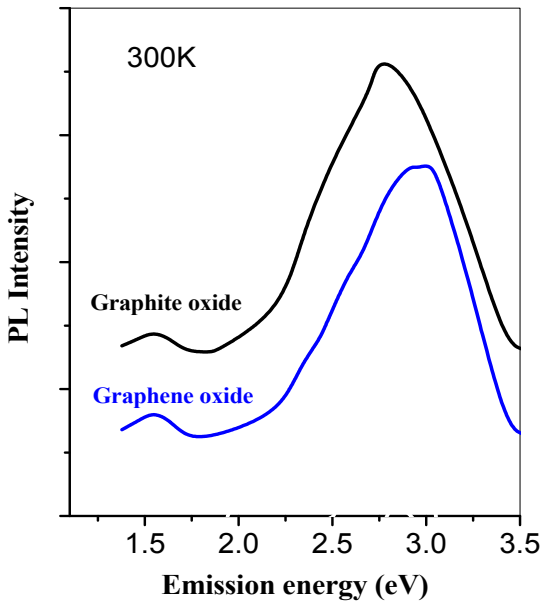

Figure 5. PL spectra of graphene and graphite oxides [25].

PL spectra of graphene and graphite oxides [25] are presented in figure 5 for the comparison. The corresponding PL peaks are: 2.79 eV for the graphite oxide and 2.95 eV for the graphene oxide. Hence the new high energy PL band B (2.88 eV) in the studied mixture is located closer to the PL

peak of graphene oxide (2.95 eV) at the end of the second MP stage. At long time of MP the peak of the new PL band B shifts to 2.85 eV closer to the graphite oxide. Note that the graphite (graphene) oxides can be created at the oxidation of carbon nanoparticles or graphene layers on the ZnO surface during prolonged MP. To make the conclusion concerning the nature of 2.85–2.88 eV PL bands the additional study is necessary.

5. Conclusion

The transformations of PL and Raman scattering spectra, and SEM images of ZnO + 3% C NC mixtures at mechanical processing have been investigated. Three stages of PL spectrum transformation have been revealed and discussed. It is shown that the first MP stage is connected with intensity quenching all PL bands owing to amorphizating the ZnO NC surface together with appearing the nonradiative recombination centers. The second MP stage is characterized by the formation of the graphene layers on the ZnO NC surface that leads to surface passivating, NR center annihilating together with slowing the PL decay kinetics at MP. Simultaneously, the new PL band peaked at 2.88 eV has appeared in PL spectra. The PL band B (2.85–2.88 eV) is attributed to emission of graphene (graphite) oxides which are formed on the second and third MP stages.

Note, that the 3–9 min MP regime, which is accompanied by graphene layer covering the ZnO NC surface, may be interesting for ZnO NC conductivity increasing in future ZnO NC applications as UV sensitive photodiodes or solar cells.

Acknowledgement

The authors would like to thank the SIP-IPN, Mexico (project 20150601) for the financial support and the CNMN–IPN for the SEM study.

Conflict of Interest

The authors declare that there are no conflicts of interest related to this study.

References

1. Pan N, Xue H, Yu M, et al. (2010) Tip-morphology-dependent field emission from ZnO nanorod arrays. *Nanotechnology* 21: 225707.
2. Park WI, Kim JS, Yi GC, et al. (2004) Fabrication and electrical characteristics of high-performance ZnO nanorod field-effect transistors. *Appl Phys Lett* 85: 5052.
3. Hsu HS, Tung Y, Chen YJ, et al. (2011) Defect engineering of room-temperature ferromagnetism of carbon-doped ZnO. *Phys Status Solidi* (RRL) 5: 447–449.
4. Hu Y, Chen H-J (2007) Origin of green luminescence of ZnO powders reacted with carbon black. *J Appl Phys* 101: 124902.
5. Katumba G, Olumekor L, Forbes A, et al. (2008) Optical, thermal and structural characteristics of carbon nanoparticles embedded in ZnO and NiO as selective solar absorbers. *Sol Energy Mater Sol Cells* 92: 1285–1292.

6. Williams G, Kamat PV (2009) Graphene−Semiconductor Nanocomposites: Excited-State Interactions between ZnO Nanoparticles and Graphene Oxide. *Langmuir* 25: 13869.
7. Kaftelen H, Ocakoglu K, Thomann R, et al. (2012) EPR and photoluminescence spectroscopy studies on the defect structure of ZnO nanocrystals. *Phys Rev* 86: 014113.
8. Torchynska TV, Sheinkman MK, Korsunskaya NE, et al. (1999) OH Related Emitting Centers in Interface Layer of Porous Silicon. *Physica B* 273–274: 955–958.
9. Korsunskaya NE, Torchinskaya TV, Dzhumaev BR, et al. (1996) Dependence of the photoluminescence of porous silicon on the surface composition of the silicon fibers. *Semiconductors* 30: 792–796.
10. Torchynska TV, Palacios Gomez J, Polupan G, et al. (2000) Complex nature of the red photoluminescence band and peculiarities of its excitation in porous silicon. *Appl Surf Sci* 167: 197–204.
11. Torchynska TV, El Filali B (2014) Size dependent emission stimulation in ZnO nanosheets. *J Lumines* 149: 54–60.
12. Tuinstra R, Koenig JL (1970) Raman spectrum of graphite. *J Chem Phys* 53: 1126–1131.
13. Kudin KN, Ozbas B, Schniepp HC, et al. (2008) Raman spectra of graphite oxide and functionalized graphene sheets. *Nano Lett* 8: 36–41.
14. Djurišic AB, Ng AMC, Chen XY (2010) ZnO nanostructures for optoelectronics: material properties and device applications. *Prog Quant Electron* 34: 191–259
15. Diaz Cano AI, El Filali B, Torchynska TV, et al. (2013) ‘‘White’’ emission of ZnO nanosheets with thermal annealing. *Physica E* 51: 24–28.
16. Liu X, Wu X, Cao H, et al. (2004) Growth mechanism and properties of ZnO nanorods synthesized by plasma-enhanced chemical vapor deposition. *J Appl Phys* 95: 3141–3147.
17. Qiu J, Li X, He W, et al. (2009) The growth mechanism and optical properties of ultralong ZnO nanorod arrays with a high aspect ratio by a preheating hydrothermal method. *Nanotechnology* 20: 155603.
18. Diaz Cano AI, El Falali B, Torchynska TV, et al. (2013) Structure and emission transformation in ZnO nanosheets at thermal annealing. *J Phys Chem Solids*74: 431–435.
19. Garces NY, Wang L, Bai L, et al. (2002) Role of copper in the green luminescence from ZnO crystals. *Appl Phys Lett* 81: 622–624.
20. El Filali B, Torchynska TV, Diaz Cano AI (2015) Photoluminescence and Raman scattering study in ZnO:Cu nanocrystals. *J Lumines* 161: 25–30.
21. Janotti A, Van de Walle CG (2009) Fundamentals of zinc oxide as a semiconductor. *Rep Prog Phys* 72: 126501
22. Reshchikova MA, Morkoc H, Nemeth B, et al. (2007) Luminescence properties of defects in ZnO. *Physica B* 401–402: 358–361.
23. Zhang DH, Xue ZY, Wang QP (2002) The mechanisms of blue emission from ZnO films deposited on glass substrate by rf magnetron sputtering. *J Phys D Appl Phys* 35: 2837–2840.
24. Singh G, Choudhary A, Haranath D, et al. (2012) ZnO decorated luminescent graphene as a potential gas sensor at room temperature. *Carbon* 50: 385–394.
25. Chien CT, Li SS, Lai WJ, et al. (2012) Tunable photoluminescence from graphene oxide. *Angew Chem Int Ed* 51: 6662–6666.

26. Liu F, Cao Y, Yi M, et al. (2013) Thermostability, photoluminescence, and electrical properties of reduced graphene oxide–carbon nanotube hybrid materials. *Crystals* 3: 28–37.

AIMS Press